Journal of Magnetic Resonance **153,** 56–68 (2001)
doi:10.1006/jmre.2001.2426, available online at http://www.idealibrary.com on IDEAL®

Dephasing Relaxation of the Electron Spin Echo of the Vibronic $Cu(H_2O)_6$ Complexes in Tutton Salt Crystals at Low Temperatures

S. K. Hoffmann,[1] J. Goslar, W. Hilczer, M. A. Augustyniak-Jabłokow, and S. Kiczka

Institute of Molecular Physics, Polish Academy of Sciences, Smoluchowskiego 17, PL-60179 Poznań, Poland

Received March 27, 2001; revised August 7, 2001; published online October 5, 2001

Two-pulse electron spin echo (ESE) measurements of the phase relaxation (phase memory time T_M) were performed in a series of Tutton salt crystals $M_2^{\mathrm{I}}M^{\mathrm{II}}(SO_4)_2 \cdot 6X_2O$ ($M^{\mathrm{I}} = NH_4$, K, Cs; $M^{\mathrm{II}} =$ Zn, Mg; $X =$ H, D) weakly doped with Cu^{2+} ions ($c \approx 10^{18}$ ions/cm^3) in temperature range 4–60 K where ESE signals were detectable. The ESE decay was strongly modulated with proton (or deuteron) frequencies and described by the decay function $V(2\tau) = V_0 \exp(-b\tau - m\tau^2)$ with the $m\tau^2$ term being temperature independent and negligible above 20 K. Various mechanisms leading to the τ- or τ^2-type ESE decay are reviewed. The m and b coefficients for nuclear spectral diffusion (NSD), electron spectral diffusion (SD), and instantaneous diffusion (ID) were calculated in terms of existing theories and the resulting rigid lattice T_M^0 times were found to be close one to another within the crystal family with average values: 17.5 μs (NSD protons), 200 μs (NSD deuterons), 8 μs (SD), and 5 μs (ID). The ID dominates but the calculated effective T_M^0 is longer than the experimental $T_M^0 = 2$ μs. This is due to a nonuniform distribution of the Cu^{2+} ions with a various degree of the disorder in the studied crystals. The acceleration of the dephasing rate $1/T_M$ with temperature is due to the mechanisms producing $\exp(-b\tau)$ decay. They are reviewed and two of them were found to be operative in Tutton salt crystals: (a) Excitations to the vibronic levels of energy Δ leading to the temperature dependence $1/T_M = B \exp(-\Delta/kT)$, with the vibronic levels produced by strong Jahn–Teller effect, and (b) spin–lattice relaxation processes being effective above 50 K. Based on the Δ values being on the order of 100 cm^{-1}, the scheme of vibronic levels in the Tutton salts is presented, and the independence of the Δ on temperature proves that the adiabatic potential surface shape of Jahn–Teller active $Cu(H_2O)_6$ complexes is not affected by temperature below 65 K.

Key Words: **ESE dephasing; electron phase relaxation; Tutton salts; Cu^{2+}.**

I. INTRODUCTION

Electron spin phase relaxation is a random dephasing process that starts from a coherent spin precession state after pulse excitation of a spin system and finishes with random precession phases of individual spins. Since in EPR of diluted magnetic systems the resonance lines are inhomogeneously broadened, i.e., are formed from unresolved spin packets resulting from hyperfine coupling with distant nuclei, the dephasing consists of two processes: irreversible dephasing of individual spins and reversible dephasing of spin packets precession. The first process is faster and described by spin–spin relaxation time T_2^*, which is the characteristic time of the free induction decay (FID). This decay is hidden, in most cases, in the dead time of pulsed EPR spectrometers (on the order of 70 ns). The second process is due to the difference in Larmor frequency of the spin packets. This process is not a true relaxation process, since it is reversible by a second resonance pulse with subsequent formation of the electron spin echo (ESE) signal. The ESE signal amplitude V decreases with time after excitation and in two-pulse experiments the ESE decay can be often described with exponential function $V(2\tau) = V_0 \exp(-2\tau/T_M)$, where τ is an interval between the exciting and refocusing pulses. The characteristic time T_M is called the phase memory time or phase storage time. The T_M, its temperature dependence, and the decay function are determined in pulsed EPR experiments using ESE signals.

Our understanding of the processes and mechanisms leading to the ESE decay is not fully satisfactory. Many of them, but not all, are well treated theoretically and experimentally verified. A simpler situation seems to exist in liquids and viscous media, where theoretical descriptions of the rotational diffusion based on the time-dependent stochastic Liouville formalism developed by Freed and co-workers well described experimental results (*1*). Another approach was proposed by the Novosibirsk group (*2, 3*) for spin dephasing in solids produced by fluctuating local magnetic fields and described by various model dynamical processes. Both approaches are still being developed but the main theoretical interest is currently shifted to the vibrational and electronic dynamics studied in vibrational echo (*4*) and optical photon echo (*5, 6*) experiments, where the old ideas from magnetic resonance found new formulations.

A specific feature of pulsed EPR experiments of paramagnetic ions is that only part of the spin system can be excited by microwave pulses. This is limited by the pulse spectral width, which for an 8-ns pulse is 2.23 mT (for $g = 2$). The excited

[1] To whom correspondence should be addressed. Fax: (+48-61)8684524. E-mail: skh@ifmpan.poznan.pl.

1090-7807/01 $35.00

spins (spins A) being in the coherent precession can form an ESE signal after the refocusing pulse. The nonexcited spins B do not take part in forming the ESE signal but can produce ESE decay when they are coupled to spins A. Generally, the number of spins that are able to form ESE signals decreases with time after excitation due to a decrease in the number of spins A by spin diffusion and/or by random changes in the precession phase via spectral diffusion or instantaneous diffusion. A change in the phase can occur as a result of dipolar coupling described by flip-flop terms $(S_1^+ S_2^- + S_1^- S_2^+)$ in the dipolar Hamiltonian. Moreover, every transition between electron energy levels due to a random time-dependent process produces a random precession phase.

Various processes and mechanisms of the electron spin phase relaxation are summarized in Fig. 1 together with their characteristic parameters influencing the ESE decay function $V(2\tau)$, where 2τ is time where the ESE signal is centered. These parameters include spin concentration c, temperature T, and τ^k being the index of exponential decay function $V(2\tau) = V_0 \exp(-a\tau^k)$.

Because of the many contributions to the effective decay function $V(2\tau)$, differentiation between various mechanisms and processes is not easy in general. However, for sufficiently low concentrations of paramagnetic centers c the contributions depending on c can be negligible or dominated by other mechanisms. Such a situation is expected for $c < 10^{18}$ spin/cm^3 in crystals with a uniform distribution of paramnetic centers.

However even in such cases an analysis of experimental ESE decays is complicated because in the most solids the decay is modulated by a few frequencies from a weak dipolar coupling to surrounding magnetic nuclei, and the ESE decay function is

$$V(2\tau) = V_{\text{decay}} \cdot V_{\text{modul}}. \qquad [1]$$

Mechanisms and processes of relaxation are mutually independent; thus,

$$V_{\text{decay}} = V_{\text{spin diff}} \cdot V_{\text{ID}} \cdot V_{\text{SD}} \cdot V_{\text{NSD}}, \qquad [2]$$

where $V_{\text{spin diff}}$ is a contribution from electron diffusion, V_{ID} is a contribution from instantaneous diffusion, V_{SD} is a contribution from electron spectral diffusion and is a product of a few mechanisms, and V_{NSD} results from nuclear spectral diffusion within proton or other nuclei systems. The V_{decay} must be subtracted from experimental decay, which is not an easy task. In this paper we will show the best and simplest way to obtain V_{decay} for a case of strong modulations.

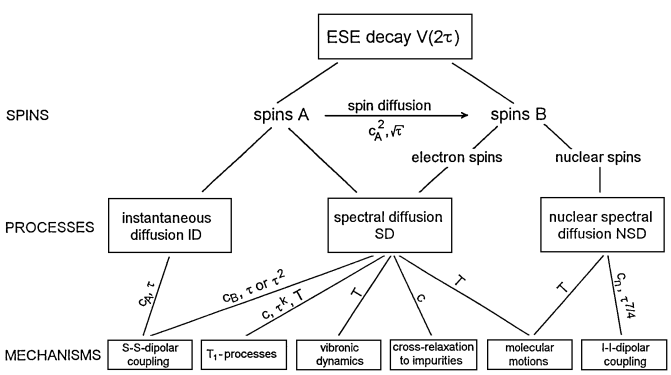

FIG. 1. Diagram of the electron spin phase relaxation processes and mechanisms with their characteristic parameters determining the decay function $V(2\tau)$: c, concentration; τ, interpulse interval; T, temperature.

This paper describes the results of the phase relaxation measurements in weakly Cu^{2+}-doped Tutton salt crystals in the low-temperature range (below 60 K) where ESE signals were detectable. We were able to identify six contributions to the decay function dominant in various temperature ranges. They are nuclear spectral diffusion NSD, instantaneous diffusion ID, electron spectral diffusion SD, vibronic dynamics, T_1 processes, and a contribution resulting from a nonuniform distribution of Cu^{2+} ions. These contributions are discussed in terms of existing theories, crystal and molecular structure, and vibronic dynamics of $Cu(H_2O)_6$ complexes.

Tutton salts form a family of $M_2^{\text{I}} M^{\text{II}}(SO_4)_2 \cdot 6H_2O$ compounds with a very similar molecular and crystal structure containing two molecules in a monoclinic unit cell (*7*). Copper(II) introduced to those crystals substitute divalent cations M^{II} (like Zn, Mg), and $Cu(H_2O)_6$ complexes undergo a strong Jahn–Teller effect. The crystal structure around the Cu^{2+} ion located at (0,0,0) and $(\frac{1}{2},\frac{1}{2},0)$ positions, with lobes of the $x^2 - y^2$ ground state, is shown in Fig. 2. The Jahn–Teller effect interplays with local crystal stress, produced by the $H_2O \ldots SO_4$ hydrogen bonds, in deformation of the hexahydrate octahedra. As a result a strong deformation appears and the adiabatic potential surface has the three potential wells with different depths. At temperatures below the room temperature only the two low energy wells are populated, and the dynamic Jahn–Teller effect is due to the jumps between these two wells corresponding to the two longest Cu–O bonds (*8*). This dynamics as well as excitations to the higher vibronic levels can influence electron spin relaxation.

We have found that the electron spin–lattice relaxation of Cu^{2+} in Tutton salt-type crystals is practically insensitive to the vibronic dynamics and is governed by ordinary two-phonon Raman processes in an intermediate temperature range (*9–12*). Phase relaxation seems to be more sensitive to the vibronic and lattice dynamics. It is due to the fact that the spin packets forming inhomogeneously broadened EPR lines are very narrow (less than 0.01 mT); thus they are easily influenced by the dynamics.

In this paper we show and discuss results for the phase memory time T_M measurements for Cu^{2+} in $(NH_4)_2Zn(SO_4)_2 \cdot 6H_2O \equiv (NH_4)_2Zn$, its deuterated analogue $(ND_4)_2Zn(SO_4)_2 \cdot 6D_2O \equiv (ND_4)_2Zn$; $K_2Zn(SO_4)_2 \cdot 6D_2O \equiv K_2ZnD$, and $(ND_4)_2Mg(SO_4)_2 \cdot 6D_2O \equiv (ND_4)_2Mg$. These data will be compared

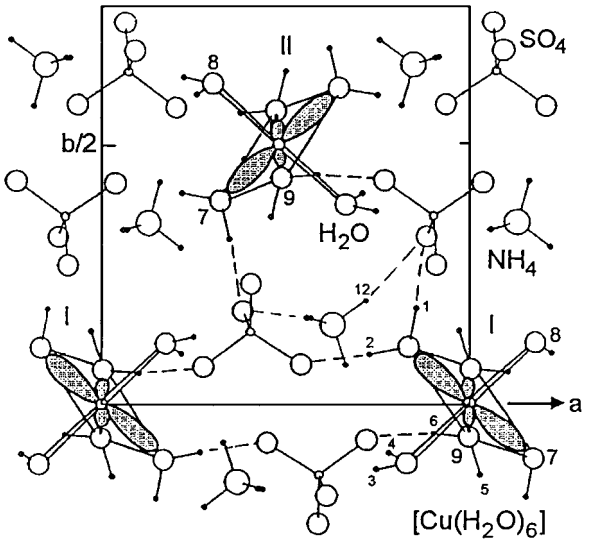

FIG. 2. Projection of the $(NH_4)_2Mg(SO_4)_2 \cdot 6H_2O$ crystal structure on the *ab* plane. Unit cell at room temperature: $P2_1/a$; $a = 0.9316$, $b = 1.2596$, $c = 0.6198$ nm, $\beta = 107.09°$, $Z = 2$, $V = 0.695 \times 10^{-21}$ cm^3. Two magnetically inequivalent positions I and II for doped Cu^{2+} ions are shown with labels of the d_{x2-y2} ground state. $Cu(H_2O)_6$ octahedra are elongated along Cu–O(7) directions. The shortest dipolar contact between protons of H_2O and NH_4, strongly influencing nuclear spectral diffusion is between $H_1(H_2O)$–$H_{12}(NH_4) = 0.259$ nm and $H_4(H_2O)$–$H_6(H_2O) = 0.266$ nm along the *c* axis.

with previously published results for $(NH_4)_2Mg(SO_4)_2 \cdot 6H_2O \equiv (NH_4)_2Mg$ (*9*, *10*), $Cs_2Zn(SO_4)_2 \cdot 6H_2O \equiv Cs_2Zn$ (*11*), and $K_2Zn(SO_4)_2 \cdot 6H_2O \equiv K_2Zn$ (*12*) to identify the dephasing mechanisms and to draw general conclusions concerning the dephasing relaxation in vibronic systems with inequivalent potential wells.

All equations used in this paper are written in SI units.

II. EXPERIMENT

1. Materials

Single crystals of Tutton salts were grown from water solutions of commercially available high-purity materials. The materials were additionally purified chemically and by several recrystallizations to remove Mn^{2+} and Fe^{3+} ions that build up very easily in crystal lattices of Tutton salt, and cross relaxation can be produced to intentionally introduce Cu^{2+} ions. Deuteration of the crystals was achieved by a fivefold recrystallization from heavy water. The degree of deuteration was determined from the peak intensity in ENDOR-type three-pulse ESEEM spectra of Cu^{2+}-doped crystals (Fig. 3). As much as 79% of ^2H was found in $(ND_4)_2Zn(SO_4)_2 \cdot 6D_2O$ with a very similar value for $(ND_4)_2Mg(SO_4)_2 \cdot 6D_2O$. In $K_2Zn(SO_4)_2 \cdot 6D_2O$ crystals the ESEEM spectrum has shown peaks from ^2H only, indicating practically total replacement of hydrogen atoms by deuterium atoms. It shows that in ammonium salts we have the fully deuterated water molecules and partially deuterated (NH_xD_{4-x}) groups with $x = 0, 1, 2, 3, 4$.

The crystals were doped with a $^{63}Cu^{2+}$ isotope by adding of about 0.1% mol of copper sulfate to the mother solution. The resulting concentration of Cu^{2+} ions in single crystals was not identical and was determined by EPR with respect to the Ultramarine Blue standard as 1.2×10^{18}–8×10^{18} ions/cm^3. Final crystallization of the compound was performed very slowly from highly uniform solutions to allow a uniform distribution of Cu^{2+} ions in the growing crystals.

2. Pulsed EPR Measurements

Electron spin echo experiments were performed on a Bruker ESP380E FT/CW spectrometer with a TE_{001} dielectric resonator and an Oxford CF935 flow helium cryostat. Relaxation measurements were carried out with the magnetic field applied along the elongation direction of $Cu(H_2O)_6$ octahedra, i.e., along the local *z* axis of the *g* and *A* tensors with excitation of the low-field $m_I = -\frac{3}{2}$ hyperfine line, which was well separated from other hyperfine lines. High resolution and the relatively narrow lines in this crystal orientation were the reason that Cu^{2+}-doped Tutton salt crystals were used for testing new methods in the pulsed EPR technique (*13*). The line was excited with 16- or 24-ns pulses in protonated compounds and with 240-ns pulses for K_2ZnD crystals having very narrow lines. The FID signal was not observed. The electron spin echo signal of the Hahn type was generated with two identical pulses with initial 120–240-ns intervals. The microwave power was adjusted to maximize the ESE amplitude, i.e., to obtain the $2/3\pi$ pulses. Thus we used the pulse sequence $2/3\pi$–τ–$2/3\pi$–τ– echo.

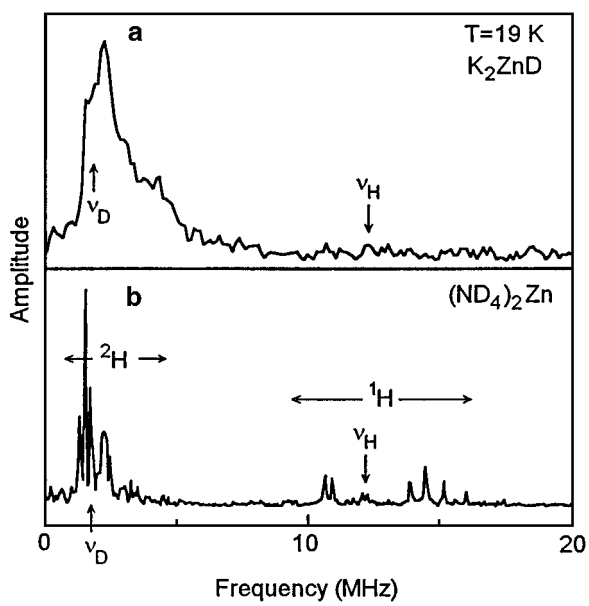

FIG. 3. Three-pulse FT-ESE spectra (ESEEM spectra) of deuterated crystals: (a) $K_2Zn(SO_4) \cdot 6D_2O$ showing full deuteration and (b) $(ND_4)_2Zn(SO_4) \cdot 6D_2O$ showing 79% deuteration with partially deuterated ammonium groups. The temperature ESE decay was measured with $\tau = 136$ ns (τ is the interval between the first two pulses) and $B = 283.6$ mT at $T = 18.5$ K.

The existence of spectral and/or instantaneous diffusion effects was checked during electron spin–lattice measurements. T_1 time dependence on microwave power and pulse length was also checked. Details of the T_1 measurements can be found in (*9–12*). The samples showing strong dependence were discarded as displaying a nonuniform distribution of Cu^{2+} ions.

Pulse EPR experiments were performed in the temperature range 4–60 K. The ESE signals were not detectable at higher temperatures because of shortening of the T_M relaxation time.

III. RESULTS

1. Electron Spin Echo Decay

Two-pulse ESE decay was strongly modulated with proton (or deuterium) frequencies of surrounding ammonium groups and water molecules. The modulation pattern was very similar for all Tutton salt crystals. Typical low-temperature decays for $(NH_4)_2Zn$ and $(ND_4)_2Zn$ are shown in Fig. 4. Modulations make it difficult to determine the decay function. A computer program effectively able to separate the modulation and decay function in $V(2\tau) = V_{\text{mod}} \cdot V_{\text{decay}}$ is not available, and we use a simple linear anamorphosis method to find V_{decay}. In most cases the plot through the upper peaks of an experimental decay $V(2\tau)$ is used as a good approximation for V_{decay}. This does not allow us, however, to distinguish clearly between exponential decay functions $V_{\text{decay}} = V_0 \exp(-m\tau^k)$ with various power coefficients k ($k_{\text{theory}} = 0.5$–3). The better way is to fit an appropriate decay function to the peaks on a semilog scale: $\log(V)$ vs τ^k (Chaps. 3 and 5 in (*2*)), (*14*). This is shown in Fig. 5 for the $(NH_4)_2Zn$ crystal with experimental decay presented in Fig. 4a. The plot

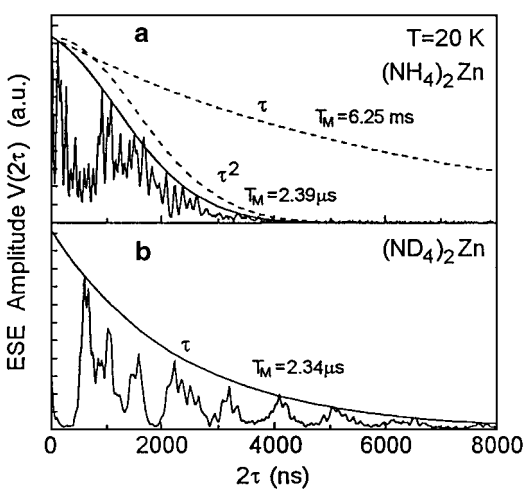

FIG. 4. Electron spin echo decay at 20 K for: (a) $(NH_4)_2Zn(SO_4) \cdot 6H_2O : Cu^{2+}$ and (b) $(ND_4)_2Zn(SO_4) \cdot 6D_2O : Cu^{2+}$. The modulated decay is approximated by $V(2\tau) = V_0 \exp(-b\tau - m\tau^2)$ function (solid lines) with $m = 0$ for deuterated compounds. Both contributions are plotted by dashed lines in (a). Phase memory time T_M values are shown for both contributions.

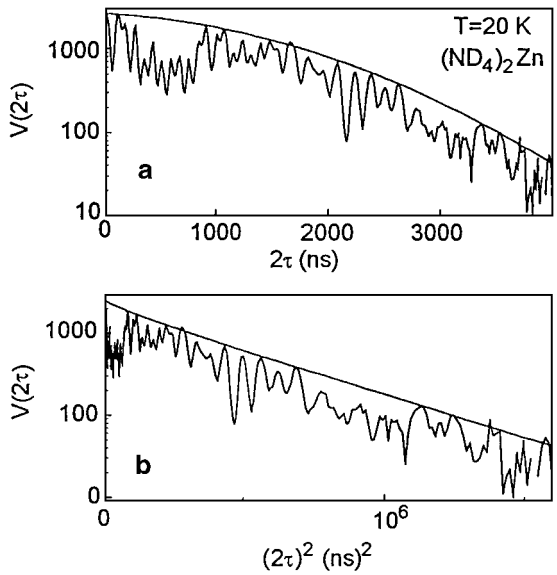

FIG. 5. Plots of the ESE decay from Fig. 4a in semilog scales. Linearity of the plot in (b) clearly shows that decay function is dominated by $\exp(-m\tau^2)$ decay.

$\log(V)$ vs 2τ in Fig. 5a clearly shows that $k \neq 1$, whereas a linear plot is seen for $k = 2$ in $\log(V)$ vs $(2\tau)^2$ (Fig. 5b). Detailed analysis has shown that a small contribution from $\exp(-b\tau)$ to $\exp(-m\tau^2)$ also exists, giving a small deviation from the straight line for small $(2\tau)^2$ values. The separated linear and quadratic contributions and the total decay function are drawn in Fig. 4a. Similar situations have been found in the other Tutton salt crystals. Thus the decay function has the form

$$V(2\tau) = V_0 \exp(-b\tau - m\tau^2). \qquad [3]$$

For the deuterated salts we found $m = 0$, whereas in protonated salts the $m\tau^2$ dominates below 20 K with the m coefficient being temperature independent. The linear term dominates at higher temperatures since the b coefficient grows with temperature in all the crystals studied.

For a multicomponent decay the phase memory time is generally defined as the time where $V(2\tau)$ falls down to the V/e value, but when various contributions can be separated then the T_M can be calculated as $T_M = m^{-1/k}$ for the $V(2\tau)$ function and as $T_M = 2m^{-1/k}$ for the $V(\tau)$ function (as obtained directly from the Bruker spectrometers). T_M values at the rigid lattice limit (below 20 K), where $k = 2$ decay dominates, are very similar for all the crystals studied with $T_M^0 = 2$–5 μs except for $(NH_4)_2Mg$, where $T_M^0 = 0.3$ μs. This latter case seems to be a result of a nonuniform distribution of Cu^{2+} ions in this crystal.

2. Temperature Dependence of the T_M Time

T_M is constant and nearly the same for all Tutton salt crystals below about 20 K, but varies with different rates at higher

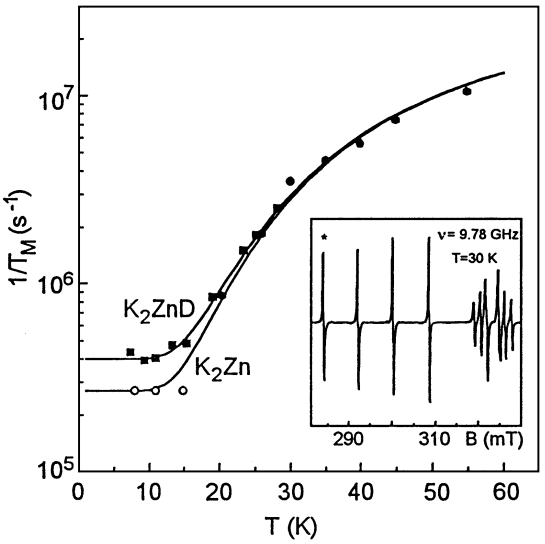

FIG. 6. Temperature dependence of the phase relaxation rate $1/T_M$ for $K_2Zn(SO_4)_2 \cdot 6H_2O : Cu^{2+}$ and $K_2Zn(SO_4)_2 \cdot 6D_2O : Cu^{2+}$ crystals. Solid lines are the best fits to the equation $1/T_M = A + B\exp(-\Delta/kT)$ with parameters given in Table 1. The inset shows the EPR spectrum for the deuterated crystal orientation where the ESE decay was measured after pulse excitation of the $m_I = -\frac{3}{2}$ line marked by the asterisk.

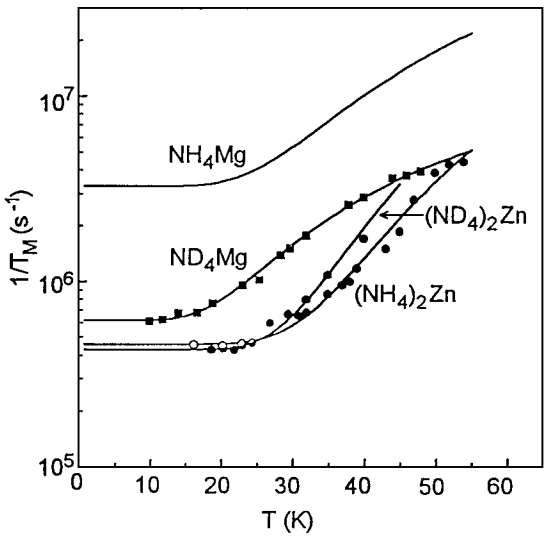

FIG. 7. Temperature dependence of the phase relaxation rate $1/T_M$ for ammonium Tutton salt crystals. The solid lines are the best fit to equation $1/T_M = A + B\exp(-\Delta/kT)$ with the parameters given in Table 1. The line without experimental points is taken from our previous paper (*9*) for comparison.

temperatures, where $k = 1$ decay dominates. Temperature variations of the relaxation rate $1/T_M$ for the potassium salts are shown in Fig. 6 and for the ammonium compounds in Fig. 7. An increase in $1/T_M$ with temperature is exponential and can be described by the equation

$$\frac{1}{T_M} = A + B\exp\left(\frac{-\Delta}{kT}\right). \qquad [4]$$

The coefficients A, B, Δ and the rigid lattice values of T_M are summarized in Table 1.

IV. DISCUSSION

In this section we discuss various mechanisms that contribute to the dephasing process, producing a decay of the perpendicular magnetization component after pulse excitations. Most of these mechanisms are not related to the Jahn–Teller effect characteristic of the $Cu(H_2O)_6$ complexes in Tutton salt crystals. Their vibronic dynamics delivers an additional, specific mechanism, producing an increase in the dephasing rate with temperature. The other mechanisms are not specific for vibronic systems and thus our discussion still applies in the absence of the Jahn–Teller effect.

We will use the theoretical results, our experimental data, and structural data to evaluate quantitatively the contributions to the total T_M value. The spin diffusion effects will not be considered.

TABLE 1

Parameters of the Temperature Dependence of the Dephasing Rate $1/T_M = A + B\exp(-\Delta/kT)$ for Cu^{2+} in Tutton Salt Crystals $M_2^{I}M^{II}(SO_4)_2 \cdot 6H_2O$

Compound $M_2^{I}M^{II}$	Concentration (spins/cm^3)	Temperature range (K)	A (s^{-1})	B (s^{-1})	Δ (cm^{-1})	T_M^0 (μs)	Ref.
K_2Zn	1.4×10^{18}	8–50	2.7×10^5	6.5×10^7	67	3.7	(*12*)
K_2ZnD	1.2×10^{18}	7–28	4.0×10^5	6.5×10^7	67	2.5	This work
$(NH_4)_2Zn$	1.6×10^{18}	16–54	4.6×10^5	38.7×10^7	169	2.2	This work
$(ND_4)_2Zn$	1.6×10^{18}	18–35	4.3×10^5	5.1×10^8	161	2.3	This work
$(NH_4)_2Mg$	4.0×10^{18}	19–53	33.0×10^5	26.6×10^7	102	0.3	(*9, 10*)
$(ND_4)_2Mg$	2.0×10^{18}	6–48	6.2×10^5	2.8×10^7	70	1.6	This work
Cs_2Zn	8.0×10^{18}	10–50	2.0×10^5	2.8×10^7	71	5	(*11*)

Note. The T_M^0 is the rigid lattice limit value $T_M^0 = 1/A$.

They are expected to produce that ESE decay $\exp(-a\sqrt{\tau})$ (*3*), which was not observed in our experiments.

The experimentally observed decay with $k = 1$ and $k = 2$ and existence of temperature dependence of the relaxation rate indicate that a few mechanisms produce the decay. Their contributions are not easy to separate in experimental results since a few mechanisms can produce $\exp(-b\tau)$ dependence, whereas the others can produce $\exp(-m\tau^2)$ decay (*2, 15*).

1. *Mechanisms Leading to the exp($-m\tau^2$) Decay*

Quadratic exponential decay is theoretically predicted for: (a) contributions from spectral diffusion of magnetic matrix nuclei (nuclear spectral diffusion) (*3, 16*); (b) electron spectral diffusion in T_2-type samples for slow electron dipolar flip-flops (*17, 18*); (c) slow electron spectral diffusion ($\tau \ll T_1$), in T_1-type samples, described by the sudden-jump (Lorentz–Markov) model of dipolar field fluctuations (*2, 19, 20*). This mechanism will be not considered below since it is not expected at low temperatures where spin–lattice relaxation is very slow with T_1 on the order of 0.1 s.

Nuclear spectral diffusion of matrix nuclei. Dipolar flip-flops of nuclear magnetic moments produce random local magnetic fields at unpaired electron sites. This fluctuating field randomly modifies the Larmor frequency of the excited electrons, leading to the dephasing of the ESE signal. The dephasing rate depends primarily on the nuclear flip-flop rate W_n and is influenced by the radius δ of the diffusion barrier. The diffusion barrier determines a sphere surrounding a paramagnetic center, where the S–I magnetic coupling is stronger than I–I magnetic coupling. The I–I flip-flops are strongly suppressed inside the sphere and these detuned spins form a frozen core around the paramagnetic center. The frozen core spins do not contribute to the dephasing since the nuclear spectral diffusion takes place only outside the frozen core. The radius δ is typically about 1 nm, and several hundred protons are frozen near paramagnetic ions in molecular crystals. The flip-flop rate is determined by the distance r between nuclei. For the average r_n distance the rate can be evaluated as (*3, 21*)

$$W_n = \left(\frac{\mu_0}{4\pi}\right)\frac{\gamma_n^2\hbar}{10r_n^3} = \left(\frac{\mu_0}{4\pi}\right)\frac{\gamma_n^2\hbar}{10}c_n \approx 10^3\text{–}10^4\ \mathrm{s}^{-1}, \qquad [5]$$

where $c_n = r_n^{-3}$ is the magnetic nuclei concentration. For short times τ the ESE decay function is (*3, 16*)

$$V(2\tau) = V_0\exp(-m_1\tau^3), \qquad [6]$$

where

$$m_1 = \left(\frac{\mu_0}{4\pi}\right)^2\frac{12\pi}{5}\gamma_n^2\gamma_e^2\hbar^2\frac{r_n^2}{\delta^5}W_nc_n.$$

Because of the strong dependence on δ the decay function for longer τ ($\tau > \delta^4/3r_n\gamma_n\gamma_e\hbar$) tends to the form

$$V(2\tau) = \exp(-m\tau^2)$$
$$m = 2\pi W_nc_n\left(\frac{\mu_0}{4\pi}3r_n\gamma_n\gamma_e\hbar\right)^{3/4}. \qquad [7]$$

We have calculated W_n and m parameters from Eqs. [5] and [7] and the resulting rigid lattice phase memory rate $1/T_M^0 = m^{1/2}$ for Tutton salt crystals using calculated concentrations of protons and deuterons $c_n =$ (number of nuclei in crystal unit cells/unit cell volume). The results are summarized in Table 2. The calculated T_M^0 times in Table 2 will be slightly longer (by a factor of about 2) when the frozen core effect is taken into account. We have not improved our calculations since the results of Table 2 compared with experimental data of Figs. 6 and 7 and Table 1 show that dephasing effects from matrix nuclei are not dominant.

Results given in Table 2 predict that the low-temperature relaxation rate for deuterons is about 10 times slower than that for protons in the same compound. Experimental data shows, however, that the dephasing rate is practically the same for protonated

TABLE 2
Nuclear Spin Flip-Flop Rate W_n and Rigid Lattice Phase Memory Time T_M^0 for Protons and Deuterons in Tutton Salt Crystals $M_2^{\mathrm{I}}M^{\mathrm{II}}(SO_4)_2\cdot 6H_2O$

			Protons ^{1}H		Deuterons ^{2}H	
Compound $M_2^{\mathrm{I}}M^{\mathrm{II}}$	c_n (spins/cm^3)	Average I–I distance (nm) r_n	Flip-flop rate W_n (s^{-1})	T_M^0 (μs)	Flip-flop rate W_n (s^{-1})	T_M^0 (μs)
K_2Zn	3.67×10^{22}	0.300	2770	19.0	—	—
K_2ZnD	3.67×10^{22}	0.300	—	—	66	248
$(NH_4)_2Zn$	5.50×10^{22}	0.263	4151	13.4	—	—
$(ND_4)_2Zn$	5.50×10^{22}	0.263	—	—	98	176
$(NH_4)_2Mg$	5.75×10^{22}	0.259	4340	12.8	—	—
$(ND_4)_2Mg$	5.75×10^{22}	0.259	—	—	101	170
Cs_2Zn	3.50×10^{22}	0.306	2642	19.8	—	—

and deuterated samples. In deuterated samples the decay function does not contain the $\exp(-m\tau^2)$ term, indicating that the matrix nuclei do not contribute to the ESE decay at all.

Electron spectral diffusion (SD) within a Cu^{2+} system. In our pulsed EPR experiments only a single hyperfine line was excited as marked by the asterisk in the inset of Fig. 6. Thus, because two quartets of hyperfine lines exist in the spectrum only 1/8 of the spins were excited (spins A). The spectral diffusion due to the dipolar coupling between nonexcited spins B can be a source of dephasing of the ESE signal formed by spins A (T_2-type samples). The problem of electron spectral diffusion in magnetically diluted paramagnets is more complicated than the matrix nuclei spectral diffusion that takes place in concentrated magnetic nuclear systems such as protons in molecular crystals. Because of a random distribution of admixtured paramagnetic centers in a crystal the unpaired spins have different environments. As a result the spin flip-flop rate is not uniquely determined, and there exists rather a distribution of flip-flop rates. A solution for the dephasing rate with distributed flip-flop rates can be obtained by the Monte Carlo method. Such an approach has been used in optical dephasing calculations (*22*) but not in ESE dephasing.

An approximate analytical solution of the problem can be found considering the most probable flip-flop rate $W_{\max}$, which is known to govern the migration of excitation energy in the luminescence damping. Assuming the Gaussian distribution of spin flip-flops, it was found that for inhomogeneously broadened EPR lines, with the total linewidth $\Delta\omega_k$ and dipolar linewidth $\Delta\omega_{1/2}$, when $\Delta\omega_k > \Delta\omega_{1/2}$ the most probable flip-flop rate is (*2, 18*)

$$W_{\max} = \left(\frac{\mu_0}{4\pi}\right)^2 \frac{2^5\pi^3}{3^6}\gamma_c^4\hbar^2 c_B^2 \frac{\Delta\omega_{1/2}}{\Delta\omega_k^2}\left(\ln\frac{\Delta\omega_k}{2\Delta\omega_{1/2}}\right)^2, \quad [8]$$

where c_B (cm^{-3}) is the concentration of spins B (1/8 of total Cu^{2+} concentration in our case). The $\Delta\omega_i$ is the half-width at half-height. The $\Delta\omega_k$ is the experimental linewidth formed by unresolved spin packets and $\Delta\omega_{1/2}$ must be calculated. The best estimation of $\Delta\omega_{1/2}$ for magnetically diluted solids with uniformly distributed paramagnetic centers was given by Abragam (*23*) as

$$\Delta\omega_{1/2} = \left(\frac{\mu_0}{4\pi}\right)3.8\gamma^2\hbar c, \quad [9]$$

whereas in various papers instead of 3.8 the values 1.5–5.3 were found, depending on the calculation method. The decay function $V(2\tau)$ of the two-pulse ESE was calculated by the Novosibirsk group (*2, 3, 18*) under assumption of the Poisson distribution of spin flip-flops,

$$V(2\tau) = V_0\exp[-4\pi \times 10^{-19}c_B Q(\tau)], \quad [10]$$

where $Q(\tau)$ was calculated numerically (*3, 17*) and c_B is the concentration of the spins B (cm^{-3}). Analytical approximations for $Q(\tau)$ were found for three ranges of $W_{\max}$, namely,

$$\text{for } W_{\max} < 10^3\ \mathrm{s}^{-1}, \quad V(2\tau) = V_0\exp\left(-\Delta\omega_{1/2}W_{\max}\tau^2\right), \quad [11]$$

$$\text{for } 10^4\ \mathrm{s}^{-1} \le W_{\max} \le 10^5\ \mathrm{s}^{-1},$$

$$V(2\tau) = V_0\exp(-5\times 10^{-19}c_B\tau), \quad [12]$$

$$\text{and for } W_{\max} > 10^6\ \mathrm{s}^{-1}, \quad V(2\tau) = V_0\exp(-b\sqrt{\tau}). \quad [13]$$

The dipolar linewidth $\Delta\omega_{1/2}$ and flip-flop rate $W_{\max}$ calculated from Eq. [9] and Eq. [8], respectively, are summarized in Table 3 for Cu^{2+} in Tutton salts. The flip-flop rates $W_{\max} \approx 10^4\ \mathrm{s}^{-1}$ are within the intermediate range where the $\exp(-m\tau^k)$ decay with $k = 1-2$ is expected, although our experimental data show $k = 2$ in the rigid lattice limit. The phase memory time calculated from Eq. [11] as $T_M^0 = 2(\Delta\omega_{1/2}W_{\max})^{1/2}$ is very close ($\pm 2\ \mu$s) to that calculated from Eq. [12] as $T_M^0 = 2(0.2\times 10^{19}c_B^{-1})$, and the average value of both is shown in Table 3. Comparison of results for T_M^0 in Tables 2 and 3 shows that the relaxation rate $1/T_M^0$

TABLE 3

Electron Spin Flip-Flop Rate $W_{\max}$ and Phase Memory Time T_M^0 Calculated for Electron Spectral Diffusion (SD) and Instantaneous Diffusion (ID) for Cu^{2+} in Rigid Lattice of Tutton Salt Crystals $M_2^{\mathrm{I}}M^{\mathrm{II}}(SO_4)_2\cdot 6H_2O$

Compound $M_2^{\mathrm{I}}M^{\mathrm{II}}$	Cu^{2+} ions				T_M^0 (μs)		
	c_S (spins/cm^3)	$\Delta\omega_k$(exp) (MHz)	$\Delta\omega_{1/2}$ (calc) (MHz)	Flip-flop rate $W_{\max}$ (s^{-1})	SD	ID	exp
K_2Zn	1.4×10^{18}	13.5	1.74	5159	10.7	6.1	3.7
K_2ZnD	1.2×10^{18}	7.7	1.49	4892	2.5	7.2	2.5
$(NH_4)_2Zn$	1.6×10^{18}	19.0	1.98	5180	10.0	5.4	2.2
$(ND_4)_2Zn$	1.6×10^{18}	10.9	1.98	6561	9.4	5.4	2.3
$(NH_4)_2Mg$	4.0×10^{18}	31.6	2.48	5110	8.5	4.3	0.3
$(ND_4)_2Mg$	2.0×10^{18}	15.4	2.48	8054	7.6	4.3	1.6
Cs_2Zn	8.0×10^{18}	14.8	4.96	8699	4.8	2.2	5.0

Note. The $\Delta\omega_i$ are half-widths at half-height as defined in the text.

for SD is only slightly slower than that for the nuclear spectral diffusion of matrix protons. The effective T_M^0 produced by these two mechanisms can be calculated (assuming $\exp(-m\tau^2)$-type decay for both) as

$$T_M^0 = \left[T_{SD}^2 \cdot T_{NSD}^2 / \left(T_{SD}^2 + T_{NSD}^2\right)\right]^{1/2},$$

which for the $(NH_4)_2Zn$ crystal with $T_{SD} = 20$ μs and $T_{NSD} = 13.4$ μs gives $T_M^0 = 11.1$ μs, which is about five times longer than the experimental T_M^0 value (see Table 1). Thus there exists an additional contribution that is also temperature independent, gives $\exp(-b\tau)$-type decay, and dominates in the deuterated crystals.

2. Mechanisms Leading to the exp(−bτ) Decay

Exponential ESE decay with the linear index τ is observed in our experiments as dominating at temperatures above 20 K. Such a type of decay is generally assumed as a good approximation in strongly modulated decays. Existing theories predict that such decays can appear at least for the following five cases: (a) for intermediate electron spectral diffusion (SD) with spin flip-flop rates in the range 10^4–10^5 s^{-1} as described above; (b) for instantaneous diffusion (ID) produced by the second pulse (*24*); (c) in T_1-type samples when spin–lattice relaxation processes are fast enough to produce effective dephasing (this effect was modeled with Markov processes assuming uncorelated spin jumps with Lorentzian frequency distribution, see p. 51 in (*2*)); (d) for fast spectral diffusion under dynamical EPR line-narrowing conditions described by the Gaussian distribution of the local magnetic fields (*20*) (see p. 40 in (*2*)); and (e) when paramagnetic centers are involved in an exchange-type process between two frequencies (*25*) (see p. 49 in (*2*)). The mechanisms (c), (d), and (e) are temperature dependent and will be described in the next section.

Instantaneous diffusion (ID). Phase relaxation of electron spins can be due to the refocusing pulse acting on the on-resonance spins A. This second pulse in a two-pulse sequence reverses spins A in the perpendicular magnetization plane. The resulting perturbation of the dipolar coupling between A spins is a source of spin precession phase randomization (*17*). This mechanism is expected to dominate over the spectral diffusion when the dipolar spin flip-flop rate is in the intermediate or slow range ($W_{max} < 10^4\ s^{-1}$). A characteristic feature of the instantaneous diffusion mechanism is the dependence on the concentration of A spins and on the magnetization turning angle $\theta = \gamma_e B_1 t_p$ (t_p is the pulse duration) (*3*, *26*)

$$V(2\tau) = V_0 \exp(-2b\tau), \qquad [14]$$

where (*3*)

$$b = \Delta\omega_{1/2} \left\langle \sin^2 \frac{\theta}{2} \right\rangle \qquad [15]$$

and the average $\langle\ \rangle$ is taken over the Larmor frequency distribution in the EPR spectrum. The b coefficient depends on the total unpaired spin concentration c, which is hidden in the expression $\Delta\omega_{1/2} = 3.8(\mu_0/4\pi)\gamma_c^2 \hbar c$, and depends on the concentration of A spins hidden in $\langle \sin^2 \theta/2 \rangle$. Brown (*20*) has shown that for Hahn-type ESE excited by two very selective $2\pi/3$ pulses $b = \Delta\omega_{1/2} c_A/c$ when $\omega_1 < \Delta\omega_k$. In our calculations we have used an approximation of the $\langle \sin^2 \theta/2 \rangle$ useful for our experimental conditions where the whole hf line was excited by two $2\pi/3$ pulses

$$b = \Delta\omega_{1/2} \frac{c_A}{c} \sin^2 \frac{\theta}{2} \qquad [16]$$

with $\sin^2 \theta/2 = 3/4$.

A more general approach describing the ID mechanism in $2+1$ pulse experiments was presented by Kurshev and Ichikawa (*24*) with

$$V(2\tau) = V_0 \exp\left(-\frac{\mu_0}{4\pi} D_A \gamma_e^2 \hbar C \sin^2 \frac{\theta}{2} \tau\right), \qquad [17]$$

where $D_A = 5.07/(1 + 1.08x^{1/2} - 2.04x + 2.51x^{3/2})$, $x = 2\omega\tau$, and the same flip-flop rate W for all the spins was assumed. The expected decay due to ID is very effective. The flips of only a small percentage of A spins will produce an observable effect (*24*). Thus SD is always accompanied by ID in the ESE decay.

Taking $\Delta\omega_{1/2}$ from Table 3 we have calculated $T_M^0(\mathrm{ID}) = 1/b$ using Eq. [16]. The results are summarized in Table 3, where the calculated phase memory times from SD and ID are compared with experimental T_M^0 values. It can be seen that ID dominates over SD and proton spectral diffusion but the experimental dephasing rate $1/T_M^0$ is still a few times faster than the calculated rates, except for the Cs_2Zn crystal having the largest Cu^{2+} concentration. Additional mechanisms that are temperature independent and can accelerate the dephasing can be related to the cross relaxation (see Fig. 1) to an impurity or to a nonuniform distribution of Cu^{2+} in the studied crystals. We claim that the latter case takes place. This effect is especially large for $(NH_4)_2Mg$ crystals, which have much a dephasing rate higher than that of $(NH_4)_2MgD$ and the other compounds (Fig. 7). A confirmation comes from our electron spin–lattice relaxation measurements in these compounds (*9*–*11*). In $(NH_4)_2Mg : Cu^{2+}$ and in $Cs_2Zn : Cu^{2+}$ at low temperatures up to about 18 K the linear term $1/T_1 = aT$ dominates spin–lattice relaxation, whereas in the other crystals this term is negligible and the ordinary two-phonon Raman processes govern the relaxation in the whole temperature range. Thus the mechanism strongly accelerating the T_1 relaxation at low temperatures and described by the aT term cannot be the direct relaxation process, which is known to give a detectable contribution below 2.1 K in Tutton salt crystals (*27*). We assume that the linear term is due to the mechanisms characteristic of disordered or amorphous solids

(*28*). They can operate when there exists a nonuniformity in the distribution of Cu^{2+} ions in Tutton salt crystals produced by noncontrolled processes during the crystal growth from water solutions.

3. Temperature-Dependent Dephasing Mechanisms

The dephasing rate increases with temperature above 20 K for Cu^{2+} ions in Tutton salt crystals. This is typical behavior observed in most ESE experiments (*29, 30*) as well as in vibrational and optical dephasing (*4*).

Spectral diffusion both in electron and in nuclear spin systems is generally assumed to be temperature independent, although it was shown recently that a weak temperature dependence of the nuclear spin flip-flops can appear as a result of internuclear distances modulation by acoustic phonons, producing phonon-assisted spin diffusion in solids (*31*). Such a temperature-dependent mechanism does not operate in our crystals since the m-coefficient in $\exp(-m\tau^2)$ decay is temperature independent. Thus different mechanisms are responsible for the observed $T_M(T)$ dependence. There are five mechanisms that can lead to an increase or decrease of the ESE dephasing rate with temperature. Two of them, mentioned at the end of the previous section, have already been analyzed theoretically. The other three, i.e., modulation of anisotropic g and A tensors by paramagnetic center motions (*32*), T_1-type processes, and thermal excitations to vibronic levels, have not been theoretically treated and we will describe them in terms of the spin packet model. This model assumes that an inhomogeneously broadened EPR line is formed from nonresolved spin packets. The spin packets in Tutton salt crystals can be identified as the unresolved hyperfine lines of distant protons that have homogeneous Lorentzian lines with the half-widths related directly to the T_M time: $\Delta\omega_{\text{packet}} = 1/T_M$. The $\Delta\omega_{\text{packet}}$ is of about 0.5 MHz in Tutton salts; thus it is comparable to the calculated dipolar linewidth $\Delta\omega_{1/2}$ (Table 2), and its temperature behavior is directly reflected in the dephasing rate.

Motional narrowing of spin packets. Thermal motions of molecules with magnetic nuclei surrounding a paramagnetic center modulate S–I dipolar coupling within the frozen core. This modulation of the local magnetic field influences the spin packet width, producing an averaging of the local field amplitude when the temperature increases. In the fast spectral diffusion limit this effect is analogous to the well-known exchange or motional narrowing effect in EPR spectra of magnetically condensed crystals. The theoretical description of this mechanism was done using a normal model of spectral diffusion (see p. 40 in (*2*)) with the resulting decay function for two-pulse ESE: $\exp(-a\tau^3)$ for the slow-diffusion limit and $\exp(-2\Delta\omega_{1/2}^2\tau_c\tau)$ at the fast-diffusion limit where τ_c is the correlation time of the molecular motions. Temperature dependence results from the temperature behavior of τ_c, which is determined by the increase of molecular motion amplitude with temperature. An increase in τ_c results in a slowing down of the dephasing rate, which, in the spin packet model, can be described as an effect of continuous spin packet narrowing due to the averaging of the local magnetic field. Such effects were observed at low temperatures for SeO_3^- radicals in $(NH_4)_2H(SeO_4)_2$ crystals (*32*).

Merging (coalescence) of spin packets. Spin packets resulting from dipolar coupling appear in pairs under an EPR line, with the splitting $\Delta\omega$ determined by the strength of the coupling. Any dynamical or exchange-type process that averages the coupling will produce an effect known as a merging (coalescence) effect in EPR spectra of exchange coupled centers. Similar effects can appear for spin packets. For slow exchange the spin packet width will continuously increase with the exchange rate, which should be observed as an acceleration of the dephasing rate. When the exchange frequency becomes comparable with the splitting $\Delta\omega$, the dephasing rate will be maximal, and a further increase in frequency will result in a decrease of the dephasing rate. Thus a resonance-type maximum in the relaxation rate should appear when $\Delta\omega \propto \omega_{ex}$. The theoretical description of this dephasing mechanism (*25*) predicts that far from the maximum range the two-pulse ESE decay will be $V = V_0\exp(-b\tau)$ with $b = 1/\tau_c$ for slow exchange and $b = -\Delta\omega\tau_c$ for fast exchange with nonexponential decay around the maximum (τ_c is the correlation time for the exchange). Maxima in $1/T_M(T)$ were observed for both paramagnetic ions and radicals in many systems (*25, 29, 30, 33, 34*), where the motional processes were identified as reorientations of the molecular group CH_3 or NH_3.

Thermal motions (jumps, rotations, librations) of a paramagnetic center with considerable g and A tensor anisotropy will produce a temperature effect opposite that from matrix molecule motions (*20*). Such motions produce time-dependent shifts $\Delta g(t)$ and $\Delta A(t)$ that increase with temperature. Resulting spin packet broadening on heating is observed as an acceleration of the dephasing rate. A similar effect is expected when T_1 processes overdominate other dephasing mechanisms as can be expected at higher temperatures. This process is generally underestimated but in our opinion it dominates in every case when $T_1 \leq 0.1\ T_M$ since the spectral diffusion has no effect when the flip rate, due to the T_1 relaxation, is comparable or higher than the dipolar flip-flop rates for electron spins weakly coupled to the crystal lattice. Experimental evidence for the dominance of the T_1 processes over the other mechanisms were found for SeO_3^- radicals in $(NH_4)_3H(SO_4)_2$ (*32*), for Cu^{2+} in SrF_2 crystals (*35*), and for Tutton salt crystals doped with Mn^{2+}, which is not a Jahn–Teller active ion. For Mn^{2+} in $(NH_4)_2Mg(SO_4)_2 \cdot 6H_2O$ crystals we found (*10*) that above 50 K $1/T_M$ continuously increases with temperature and is described by the equation $1/T_M = 1/T_M^0 + \alpha/T_1$ with $\alpha = 1.5$. Theoretical models describing this dephasing mechanism (*3, 20*) do not predict a simple exponential decay $\exp(-b\tau^k)$ with $k = 1$ but with $k = \frac{1}{2}$, 2, and $\frac{3}{2}$.

An increase in dephasing rates for Cu^{2+} in Tutton salts is seen above 20 K where T_1 is still more than two orders of magnitude

greater than T_M, whereas the T_1 influence is not expected below 50 K. This increase is described by Eq. [4] and is related to continuous spin packet broadening on heating. This is a thermally activated process with activation energy on the order of $\Delta = 100\ cm^{-1}$ as shown in Table 1. The energy Δ is consistent with the energy of the first excited vibronic level in the deepest potential well of the adiabatic potential surface of vibronic $Cu(H_2O)_6$ complexes in Tutton salts as determined from other EPR experiments. Thus we claim that the dephasing mechanism is vibronic in origin and consists of either excitations and deexcitations (Orbach-type processes) within the same potential well or excitation with subsequent tunneling to the second well. The former mechanism is specific for Jahn–Teller systems and does not opperate at all via pure vibrational levels but is allowed by a mixing of electronic and nuclear wavefunctions in the vibronic levels. The B coefficient of Eq. [4] is expected, in such a case, to be on the order of molecular vibration frequencies $10^{13}\ s^{-1}$. For the tunneling mechanism, the B coefficient is expected to be on the order of tunneling frequencies $10^{6-7}\ s^{-1}$. Thus we can assume that the vibronic dephasing mechanism is due to the phonon-controlled tunneling between potential wells via excited vibronic levels as shown by the wavy lines in Fig. 10.

Various mechanisms producing temperature dependences of the dephasing rate $1/T_M$ are shown schematically in Fig. 8.

Summarizing the dephasing mechanisms discussed above, we can write the total two-pulse ESE decay of Cu^{2+} in Tutton salt crystals as

$$V(2\tau) = V_0 \exp(-m_{\mathrm{NSD}}\tau^2 - b_{\mathrm{SD}}\tau^2 - b_{\mathrm{ID}}\tau - b_{\mathrm{vibronic}}(T)\tau) \cdot V(T_1, T) \cdot V(\mathrm{disorder}). \quad [18]$$

Various contributions to the temperature variation of the experimental dephasing rate are shown in Fig. 9 for ammonium Tutton salts.

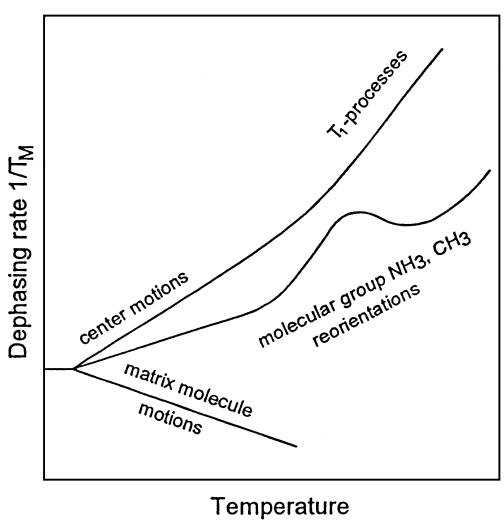

FIG. 8. Schematic presentation of various mechanisms producing temperature dependence of the dephasing rate $1/T_M$ (see text for details).

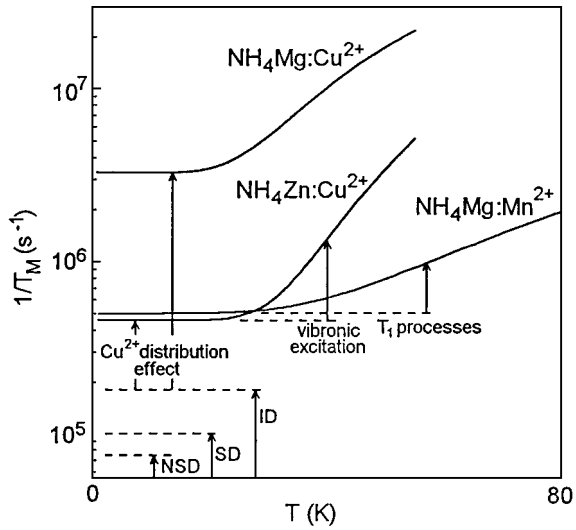

FIG. 9. Various contributions to the dephasing rate $1/T_M$ of Cu^{2+} ions in Tutton salts shown for $(NH_4)_2Mg(SO_4)_2 \cdot 6H_2O : Cu^{2+}$, Mn^{2+}, and $(NH_4)_2Zn(SO_4)_2 \cdot 6H_2O : Cu^{2+}$. SD, electron spectral diffusion; NSD, proton spectral diffusion; ID, electron instantaneous diffusion. Deuterium spectral diffusion contribution in deuterated Tutton salts is on the order of $0.5 \times 10^4\ s^{-1}$ and is not shown in the figure.

4. Vibronic Levels in Two Deepest Potential Wells of the Cu(H_2O)$_6$ Potential Surface in Tutton Salt Crystals

Knowledge of the vibronic level energy in strongly inequivalent potential wells of $Cu(H_2O)_6$ vibronic complexes in Tutton salt is of primary interest in the description of the strong Jahn–Teller effect in these compounds (*36*). Experimental determination of these energies is not possible from IR and Raman spectra because of a small concentration of doped Cu^{2+} ions, whereas for higher concentrations the cooperative elastic coupling dominated. The best method to determine δ and Δ energies (see Fig. 10) is EPR spectroscopy, supported by X-ray diffraction data and theoretical calculations (*8*). The energy differences between the wells can be determined from vibronic averaging of the g factors in EPR spectra (*8, 37–39*), and energy Δ can be experimentally found from ESE dephasing studies. These parameters are summarized in Table 4.

The values of Δ determined from our ESE measurements in this paper and in our previous papers (*9–12, 37, 38*) are generally lower than those determined indirectly from the three-level vibronic averaging model of paper (*8*) where additional assumptions of the g factor in excited vibronic levels were needed. Our data are directly determined and are of higher accuracy. The Δ values are expected to be larger for ammonium Tutton salts where the shape of the potential surface is strongly influenced by the vibronic cluster formed by a $Cu(H_2O)_6$ complex surrounded by SO_4 groups hydrogen bonded to the water molecules and by

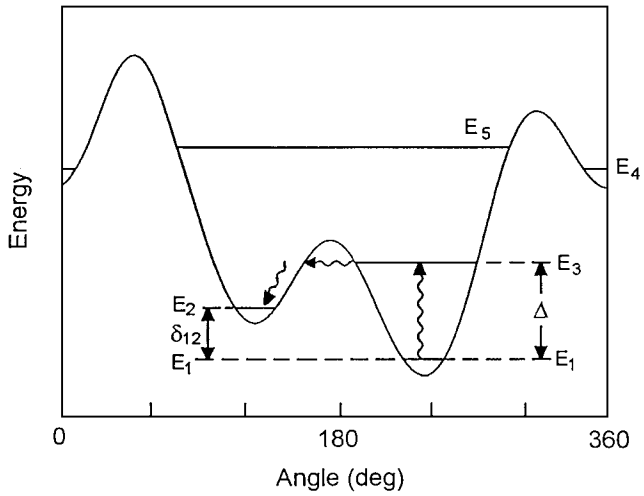

FIG. 10. An angular cross section along the Jahn–Teller radius through the adiabatic potential surface of $Cu(H_2O)_6$ complexes in Tutton salt crystals with vibronic energy levels. The energy E_4 is higher than 300 cm^{-1}; thus this level is not populated at low temperatures when our ESE experiments were performed. The wavy lines show the phonon-controlled tunneling process leading to the ESE dephasing.

NH_4 groups linked by hydrogen bonds to the SO_4 groups (*38*). The effect of the third coordination sphere formed by ammonium groups is so strong that the Jahn–Teller deformation of $Cu(H_2O)_6$ appears along Cu–O(7) in the ammonium compound, instead of Cu–O(8) as in other Tutton salts (see Fig. 2). Thus the values $\Delta = 187$ and 292 cm^{-1} for the compounds K_2Zn and Cs_2Zn, respectively, determined in (*8*) from the g-factor temperature dependence, seem to be strongly overestimated. Deuteration does not influence the Δ value in K_2Zn crystals but Δ is reduced in the ammonium compounds. This is clearly the vibronic cluster effect.

TABLE 4
Energy Difference δ_{12} between Potential Wells and Energy Δ of the First Excited Vibronic Level of $Cu(H_2O)_6$ Complexes in Tutton Salt Crystals Determined from EPR and ESE Studies

Compound $M_2^I M^{II}$	δ_{12} (cm^{-1})	Δ (cm^{-1})	Ref.
K_2Zn	68	67	(*12*)
	72	187	(*8*)
	75	—	(*39*)
K_2ZnD	—	67	This paper
Cs_2Zn	318	71	(*11*)
	235	292	(*8*)
	290	—	(*39*)
$(NH_4)_2Zn$	230	—	(39)
	181	235	(*8*)
	220	—	(*38*)
	—	169	This paper
$(ND_4)_2Zn$	—	161	This paper
$(NH_4)_2Mg$	108	102	(*9, 10*)
$(ND_4)Mg$	—	70	This paper

Comparing δ_{12} and Δ one can see that in most cases $\delta_{12} > \Delta$, whereas $\delta_{12} = \Delta$ in K_2Zn and $\delta_{12} < \Delta$ in $(NH_4)_2Mg$. These relations determine an effectiveness of interwell transitions in the dynamic Jahn–Teller effect via incoherent tuneling mechanisms at low temperatures ($T < 100$ K) and also determine a type of vibronic g-factor behavior. This behavior is perfectly described by a two-well model in K_2Zn (*12, 40*). The model works approximately only in the other compounds except for the $(NH_4)_2Mg$ crystal where it is practically invalid because the vibronic effects appear only in a relatively narrow temperature range (*9*). It should be noted, however, that this simple model works only in a restricted temperature range typically 100–200 K. It is assumed that outside of this range the adiabatic potential surface is temperature dependent. Our data clearly show, however, that this is not true below 50 K where we found Δ to be temperature independent.

V. CONCLUSIONS

Analysis of experimental data presented in this paper was done in terms of theories developed mainly by the Novosibirsk group basing on Mims' ideas (*41*). Alternative theories also exist but are applicable mainly to liquids or glass systems where disorder smears out an anisotropy of interspin interactions. The theories have been tested so far mainly in systems where ESE decay was nonmodulated or only weakly modulated by dipolar coupling to the matrix nuclei. In this paper we showed that even in the case of strong modulation it is possible to separate various contributions to the decay function after careful analysis of the $\exp(-m\tau^k)$ contributions to the decay with various k by plotting the experimental modulated decay in *semilog* scale instead of using cumbersome simulations for which computer programs are not readily available.

Quantitative analysis based on experimental Cu^{2+} concentrations and crystal structure data allowed us to calculate average dipolar flip-flop rates for unpaired electrons and matrix protons or deuterons. The calculated dephasing rate $1/T_M$ is, however, several times slower than that of the experimental results. Thus existing theories do not reproduce real results perfectly. We suppose that a disorder effect resulting from nonuniform Cu^{2+} distribution in the studied crystals should be added to obtain agreement with the experimental decay rates. Deuteration of the crystals shows that nuclear spectral diffusion has an insignificant effect on ESE decay, which is dominated by the disorder effect and the instantaneous diffusion effect. It means that the Cu^{2+} concentration on the order of 10^{18} ions/cm^3 is still too high to avoid dipolar *S–S* coupling, although the average Cu–Cu distance is then about 10 nm. The calculated T_M^0 values due to the proton spectral diffusion are the highest limit for T_M times in a rigid lattice and are on the order of $T_M(\max) \approx 20\,\mu$s.

By way of contrast to the spin–lattice relaxation, which is governed by ordinary phonon processes in Tutton salt crystals, the dephasing of spin precessional motion is sensitive

to the vibronic dynamics at low temperatures where dynamic Jahn–Teller reorientations are very slow. This provides a unique possibility to determine the energy of excited vibronic levels Δ from temperature variations of the dephasing rate.

ACKNOWLEDGMENT

This work was supported by Polish Research Scientific Council under Grant KBN-2-P03B-122-14.

REFERENCES

1. L. J. Schwartz, A. E. Stillman, and J. H. Freed, Analysis of electron spin echoes by spectral representation of the stochastic Liouville equation, *J. Chem. Phys.* **77,** 5410–5425 (1982).
2. K. M. Salikhov, A. G. Semenov, and Yu. D. Tsvetkov, "Electron Spin Echoes and Their Applications," Science, Novosibirsk (1976). [In Russian.]
3. K. M. Salikhov and Yu. D. Tsvetkov, *in* "Time Domain Electron Spin Resonance" (L. Kevan and R. N. Schwartz, Eds.), Chap. 7, Wiley, New York (1979).
4. K. D. Rector, A. S. Kwok, C. Ferrante, R. S. Francis, and M. D. Fayer, Vibrational echo studies of pure dephasing: Mechanisms in liquids and glasses, *Chem. Phys. Lett.* **276,** 217–223 (1997).
5. S. B. Altner, M. Mitsunaga, G. Zumofen, and U. P. Wild, Dephasing–rephasing balancing in photon echoes by excitation induced frequency shifts, *Phys. Rev. Lett.* **76,** 1747–1750 (1996).
6. H. Wang and S. Huang, Calculations of non-exponential photon-echo decays of paramagnetic ions in the superhyperfine limit, *Physica B* **239,** 261–266 (1997).
7. E. N. Maslen, S. C. Ridout, K. J. Watson, and F. H. Moore, The structures of Tutton salts. diammoniaium hexaaquamagnesium(II) sulphate, *Acta Crystallogr. Sect. C* **44,** 409–412 (1988).
8. M. J. Riley, M. A. Hitchman, and A. W. Mohammed, Interpretation of the temperature dependent g values of the $Cu(H_2O)_6^{2+}$ ion in several host lattices using a dynamic vibronic coupling model, *J. Chem. Phys.* **87,** 3766–3778 (1987).
9. S. K. Hoffmann, J. Goslar, W. Hilczer, M. A. Augustyniak, and M. Marciniak, Vibronic behavior and electron spin relaxation of Jahn–Teller complex $Cu(H_2O)_6$ in $(NH_4)_2Mg(SO_4)_2 \cdot 6H_2O$ single crystal, *J. Phys. Chem. A* **102,** 1697–1707 (1998).
10. S. K. Hoffmann, M. A. Augustyniak, J. Goslar, and W. Hilczer, Does the Jahn–Teller effect influence electron spin relaxation? Electron paramagnetic resonance and electron spin echo studies of the Mn^{2+} doped $(NH_4)_2Mg(SO_4)_2 \cdot 6H_2O$ single crystal and comparison with Cu^{2+} data, *Mol. Phys.* **95,** 1265–1273 (1998).
11. S. K. Hoffmann, J. Goslar, W. Hilczer, R. Kaszyński, and M. A. Augustyniak–Jabłokow, Electron spin relaxation of the Jahn–Teller $Cu(H_2O)_6$ complex in $Cs_2Zn(SO_4)_2 \cdot 6H_2O$ crystals, *Sol. State Comm.* **117,** 333–336 (2001).
12. S. K. Hoffmann, J. Goslar, W. Hilczer, and M. A. Augustyniak–Jabłokow, Electron spin relaxation of vibronic $Cu(H_2O)_6$ complex in $K_2Zn(SO_4)_2 \cdot 6H_2O$ single crystals, *J. Phys.: Condens. Matter* **13,** 1–12 (2001).
13. A. Schweiger, Creation and detection of coherence and polarization in pulsed EPR, *J. Chem. Soc., Faraday Trans.* **91,** 177–190 (1995).
14. S. A. Altshuler, I. N. Kurkin, and V. I. Shlenkin, Phase relaxation in the case of strong spin polarization, *J. Exp. Theor. Phys.* **79,** 1592–1599 (1980). [In Russian.]
15. M. Romanelli and L. Kevan, Evaluation and interpretation of electron spin-echo decay. Part I: Rigid samples, *Concepts Magn. Reson.* **9,** 403–430 (1997).
16. A. D. Milov, K. M. Salikhov, and Yu. D. Tsvetkov, Phase relaxation of atomic hydrogen in amorphous matrix, *Sov. Phys. Solid State* **15,** 802–810 (1973) [*Fiz. Tverd. Tela* **15,** 1187–1195].
17. J. R. Klauder and P. W. Anderson, Spectral diffusion decay in spin resonance experiments, *Phys. Rev.* **125,** 912–932 (1962).
18. A. D. Milov, K. M. Salikhov, and Yu. D. Tsvetkov, Effect of spin dipole-dipole interaction on phase relaxation in magnetic diluted solids, *J. Exp. Theor. Phys.* **63,** 2329–2335 (1972). [In Russian.]
19. P. Hu and S. R. Hartmann, Theory of spectral diffusion decay using an uncorrelated-sudden-jump model, *Phys. Rev. B* **9,** 1–12 (1974).
20. I. M. Brown, *in* "Time Domain Electron Spin Resonance" (L. Kevan and R. N. Schwartz, Eds.), Chap. 6, Wiley, New York (1979).
21. G. R. Khutsishvili, Spin diffusion, *Usp. Fiz. Nauk* **87,** 211–254 (1965). [In Russian.]
22. R. G. DeVoe, A. Wokaun, S. C. Rand, and R. G. Brewer, Monte Carlo theory of optical dephasing on $LaF_3 : Pr^{3+}$, *Phys. Rev. B* **23,** 3125–3138 (1981).
23. A. Abragam, "The Principles of Nuclear Magnetism," Chap. 4, Clarendon, Oxford (1961).
24. V. V. Kurshev and T. Ichikawa, Effect of spin flip-flop on electron-spin-echo decay due to instantaneous diffusion, *J. Magn. Reson.* **96,** 563–573 (1992).
25. Yu. D. Tsvetkov and S. A. Dzuba, Pulsed ESR and molecular motions, *Appl. Magn. Reson.* **1,** 179–194 (1990).
26. M. Brustolon, A. Zoleo, and A. Lund, Spin concentration in a possible ESR dosimeter: an electron spin echo study on x-irradiated ammonium tartrate, *J. Magn. Reson.* **137,** 389–396 (1999).
27. T. E. Pratt, Frequency dependence of the paramagnetic relaxation in a copper Tutton salt, *Phys. Rev. A* **177,** 664–669 (1969).
28. S. K. Misra, Spin-lattice relaxation time in amorphous materials as effected by exchange interactions, tunneling level states (TLS) centres, and fractons, *Spectrochim. Acta A* **54,** 2257–2267 (1998).
29. K. Nakagawa, M. B. Candelaria, W. W. C. Chik, S. S. Eaton, and G. R. Eaton, Electron-spin relaxation times of chromium (V), *J. Magn. Reson.* **98,** 81–91 (1992).
30. J. L. Du, G. R. Eaton, and S. S. Eaton, Electron spin relaxation in vanadyl, copper(II), and silver(II) porphyrins in glassy solvents and doped solids, *J. Magn. Reson. A* **119,** 240–246 (1996).
31. J. Dolinsek, P. M. Cereghetti, and R. Kind, Phonon-assisted spin diffusion in solids, *J. Magn. Reson.* **146,** 335–344 (2000).
32. W. Hilczer, S. K. Hoffmann, J. Goslar, J. Tritt-Goc, and M. Augustyniak, Electron spin echo studies of spin-lattice and spin-spin relaxation of SeO_3^- radicals in $(NH_4)_3H(SeO_4)_2$ crystal, *Solid State Commun.* **85,** 585–587 (1993).
33. L. D. Kispert, M. K. Bowman, J. R. Norris, and M. S. Brown, Electron spin echo studies of the internal motion of radical in crystals: phase memory vs correlation time, *J. Chem. Phys.* **76,** 26–30 (1982).
34. S. K. Hoffmann, W. Hilczer, and J. Goslar, Electron spin echo studies of flipping type minimum in phase memory time of Cu(II) ions in triglycine selenate crystal at low temperatures, *Solid State Commun.* **100,** 449–452 (1996).
35. S. K. Hoffmann and V. A. Ulanov, Off-centre dynamic Jahn–Teller effect studied by electron spin relaxation of Cu^{2+} ions in SrF_2 crystal, *J. Phys.: Condens. Matter* **12,** 1855–1866 (2000).
36. M. A. Hitchman, The influence of vibronic coupling on the spectroscopic properties and stereochemistry of simple 4- and 6-coordinate copper(II) complexes, *Comments Inorg. Chem.* **15,** 197–254 (1994).

37. S. K. Hoffmann, R. Kaszyński, M. A. Augustyniak, and W. Hilczer, Restricted validity of the two-state model describing a vibronic EPR g-factor averaging in $Cs_2Zn(SO_4)_2 \cdot 6H_2O$ Tutton salt crystals doped with Cu^{2+} ions, *Acta Phys. Pol. A* **96,** 733–740 (1999).

38. M. A. Augustyniak and A. E. Usachev, The host lattice influence of the Jahn-Teller effect of the $Cu(H_2O)_6^{2+}$ complex studied by EPR in $K_2Zn(SO_4)_2 \cdot 6H_2O$ and $(NH_4)_2Zn(SO_4)_2 \cdot 6H_2O$ Tutton salt crystals, *J. Phys.: Condens. Matter* **11**, 4391–4400 (1999).

39. V. E. Petrashen, Yu. V. Yablokov, and R. L. Davidovich, The lattice structure parameters and configuration of Cu^{2+} Jahn–Teller centers in Tutton salt crystals, *Phys. Status Solid* **101,** 117–125 (1980).

40. B. L. Silver and D. Getz, ESR of $Cu^{2+}(H_2O)_6$: A quantitative study of the dynamic Jahn–Teller effect in copper–doped zinc Tutton's salt, *J. Chem. Phys.* **61,** 638–650 (1974).

41. W. B. Mims, *in* "Electron Paramagnetic Resonance" (S. Geschwind, Ed.), Chap. 4, Plenum, New York (1972).